

# Development of a biosafety level-2 facility for irradiation of biological cells using MeV ions

Jay D. Dias<sup>a,b</sup>, Naresh T. Deoli<sup>a,b</sup>, Deborah Rogers<sup>c</sup>, Armin de Vera<sup>a</sup>, Karen M. Smith<sup>c</sup>, Robin Schneider-Broussard<sup>d</sup>, Harry J. Whitlow<sup>a,b,\*</sup>

<sup>a</sup>Louisiana Accelerator Center, University of Louisiana at Lafayette, P.O. Box 42410, Lafayette, LA 70504, USA.

<sup>b</sup>Department of Physics, University of Louisiana at Lafayette, P.O. Box 43680, Lafayette, LA 70504, USA.

<sup>c</sup>Department of Biology, University of Louisiana at Lafayette, P.O. Box 43602, Lafayette, LA 70504, USA.

<sup>d</sup>Office of Research Integrity, University of Louisiana at Lafayette, P.O. Box 43610, Lafayette, LA 70504, USA.

---

## Abstract

The development of a facility for irradiation of murine and primate tissue presents several challenges. First, extremely low fluences ( $10^6$ – $10^{11}$  ions  $\text{cm}^{-2}$ ) are required to deliver doses of 1 mGy – 50 Gy using MeV proton. Second, the tissues, particularly from non-human primate, may be infectious to humans. Third, protection of irradiated tissue samples from contamination by mold and bacteria is critical. Here we present an ultra-low flux irradiation facility and associated fluence control for biological cell and tissue irradiation under sterile biosafety level 2 (BSL-2) conditions suitable for use with low energy (1–3.4 MeV) protons. The operation is demonstrated using murine astrocytes.

**Keywords:** Ultra low-flux irradiation, MeV ion microprobe, Tissue irradiation, Biosafety, Murine astrocytes

---

## 1. Introduction

The interaction of charged particles with biological tissues is attracting much topical interest, especially for simulating the charged particle irradiation during manned long-duration deep-space missions. Biological tissue, a dense 3D matrix of cells, actively communicates by chemical, electrical, and tactile signals. A well-known example where the chemical signalling is important is the external apoptosis pathway [1]. Since this signalling will be largely absent in single-cell and low-confluence 2D cell cultures; irradiation studies of biological tissue will be an important compliment to these studies. The need to work with tissues from animal models, in particular non-human primate tissues, (which have the closest physiology to humans) presents an infection risk to the operators. In addition, the cell and tissue cultures must be protected from infection by bacteria and fungi for long periods (months) to prevent loss of samples and invalidation of entire test series. This is particularly important when multiple dose fractions need to be delivered to simulate chronic radiation exposures.

During long duration interplanetary space travel astronauts can be expected to receive cumulative radiation doses from charged particles of 5–200 cSv [2, 3]. The dose is dominated by the contribution from protons with energies of 0.1–200 MeV [4]. The energy deposition from charged particles penetrating matter is different from that for electrons, X-, and  $\gamma$ -rays. The charged particle flux will be attenuated and its energy degraded by penetration of the spacecraft walls, (typically equivalent to

$\sim 10$  g  $\text{cm}^{-2}$  Al). The penetration of the residual MeV protons in tissue has a strong maximum in the dose distribution close to the end of the range where the ions have slowed to a few MeV energy. This opens a route to study the effects of space radiation on tissue by directly irradiating cell- and tissue cultures with MeV protons. There is considerable data using rodent and rabbit animal models with GeV/u energy ions. However, the size and spatial distribution of the dose about the ion tracks is quite different for protons with  $<10$  MeV energy than ions of GeV/u energy. The dose  $D$  in a sample of density  $\rho$  and thickness  $t$  ( $<$ ion range) is related to the ion fluence  $\Theta$  according to:

$$D = \frac{\Theta}{\rho} \left( \overline{\frac{dE}{dx}} \right) \quad (1)$$

The mean stopping force  $\overline{dE/dx}$  [5] and proton fluence for a mean dose of 1 Gy in the limit of a thin film of tissue is presented in Table 1. The onset of biological effects in cells is a small fraction of 1 Gy, of the order of 10–20 cGy. This coupled with the need to deliver the radiation insult over a time that can be determined precisely, (10–1000 s) and over a number of small dose fractions implies that fluxes of  $\sim 10^6$  protons  $\text{cm}^{-2}$   $\text{s}^{-1}$  are required. The ion-optical approach presented here is an extension of previous work where an image of the illuminated objective aperture is brought to a focus and allowed to expand behind the focus to give a uniform flux over a surface behind the conjugate [6, 7]. This paper describes the development of a biosafety level-2 facility for irradiation of biological cells/tissue using low energy protons by utilising a glove box.

---

\*Corresponding author

Email address: hxw1673@louisiana.edu (Harry J. Whitlow)

## 2. Biosafety aspects

The Centers for Disease Control have specified four biosafety (or containment) levels describing the measures to be applied when working with biological agents [8]. Biosafety level-1 is suitable for agents not known to cause disease in humans. Biosafety level-2 (BSL-2), the level adopted for this work, is suitable for agents that pose a moderate risk to personnel and environment. Biosafety level-3 is used for agents that can cause potentially lethal disease via the inhalation route. Biosafety level-4 is for agents that are aerosol transmitted and have a high risk to cause fatal disease for which there is no treatment or vaccine available. NHP tissue may contain Hepatitis B, Simian immunodeficiency virus, Simian B virus, *Campylobacter*, *Salmonella*, *Shigella*, etc. [9]. Since infection via respiratory route for these is low, and vaccination or treatment are available, the BSL-2 is appropriate for handling cells and tissues from non-human primates. Several modalities in accelerator laboratories meet the general BSL-2 safety requirements [8], including controlled access and security with appropriate training of the laboratory personnel. For BSL-2, provisions must be made to decontaminate equipment and work under biocontainment when actions may create aerosols.

Accelerator laboratories are however poorly compatible with achieving a sterile environment. Nevertheless, it is not essential that the entire accelerator or target area be at BSL-2 standard. At the Louisiana Accelerator Center, tissue (cultured in BSL-2 conditions in cell and tissue culture lab [13]) will be irradiated under sterile BSL-2 conditions. The beam tube penetrating the wall of the glove box can be sealed, such that the irradiation takes place within the biocontainment (Fig. 1). The glove box is equipped with a load-lock mechanism, so the boxed samples can be maintained in a sterile environment during handling and mounting the tissue sample for irradiation. Irradiated samples will be swiftly restored into growth-media, boxed and transferred through the load-lock into a thermally insulated box. Sterilization was carried out using Sani-Plex 128m (Wilmington, DE) a disinfectant for solid surfaces. The glove box exhaust passes through scrubbers. The advantage of this approach is that the cells/tissue is maintained in a sterile environment, even though they are transferred between different laboratories.

## 3. Low-flux irradiation facility

The ion-optical approach to produce sufficiently low fluxes of ions is to first reduce the beam by collimation and then use a MeV ion microprobe to spread out the beam after the conjugate focus [6, 7]. In this work, we use an Oxford Microbeams (OM) quadrupole triplet system attached to National Electrostatic Corporation's 1.7 MeV Pelletron accelerator. Oxford Microbeam's beam defining slits OM10 [10] and a Cu plate with 2, 1, 0.5, and 0.25 mm holes served as the objective and collimator aperture, respectively. This enabled reduction of the beam flux by a precise factor in the range  $10^4$ – $10^6$ . The collimator aperture of 1 mm diameter was used to irradiate uniformly the exit

window as discussed below. The second stage of beam reduction used the microprobe optics, which were a standard OM50 quadrupole triplet in a converging-diverging-converging configuration without scanning, (Fig. 2) to produce a divergent beam that impinges on the target some distance (0.8 m) after the conjugate focus. The beam was brought out into air by means of a 200 nm thick 1 mm  $\times$  1 mm  $\text{Si}_3\text{N}_4$  membrane that contributed negligible energy loss, (0.84 keV for 2 MeV protons [5]). The energy loss in the 5 mm air gap, (Table 1) was negligible.

To optimize the design with respect to uniformity of the beam current distribution over the sample surface, WinTRAX [11], a raytracing software from OM was used. Fig. 2 (b) presents the calculated ray traces for the set-up with a 0.5 mm diameter collimator aperture and a  $16 \mu\text{m} \times 30 \mu\text{m}$  objective aperture. The source was 10% larger than the objective aperture and a symmetrical beam divergence of 0.3 mr was used. This was used to ensure the objective aperture was uniformly illuminated. Figure 3 presents the calculated beam spot flux distributions for different collimator aperture sizes using  $3 \times 10^6$  incident ions from the source. Although the intensity in the individual pixels varies, the absence of an average colour change over the irradiated areas demonstrates the ion fluence is very uniform over the 1 mm  $\times$  1 mm irradiated area (TS in Fig. 2 (a)) used in the experimental irradiations. The elliptical beam spots in Fig. 3 (b) and (c) are observed because the collimator aperture controls the angular widths of the elliptical cone of rays leaving the conjugate point and hence the size of the irradiated area on the sample. It does this by cutting away those rays that enter the lens with the largest distance from the optic axis (Fig. 2 (b)). This action is analogous to that of the condenser aperture in Köhler illumination in optical- and transmission electron-microscopes. The objective aperture acts as a field aperture that spatially samples a small area of the beam from the accelerator over which the beam-divergence and -flux is uniform at the collimator aperture. The triplet lens maps the image of the collimator aperture giving a uniform flux image at the target position [12]. The beam flux reduction factor is thus independent of the collimator size and governed by the size of the objective aperture and the inverse square flux dependence on the post-focus expansion distance. The uniform distribution of MeV ions using a post-focus expansion methodology has been reported previously [6, 7].

A fluorescent screen, Faraday cup, and a 1 mm  $\times$  1 mm and 200 nm  $\text{Si}_3\text{N}_4$  foil are mounted on a target stick at the conjugate focus position, (Fig. 2 (a)). The biological samples on microscope coverslips were mounted 5 mm behind the radiation exit membrane on a X-Y-Z stage. Two Si p-i-n charged particle detectors (Hamamatsu S1223-01 with borosilicate window removed) D1 and D2 in Fig. 2 were used to monitor the ion flux. D1 was used to measure the yield of ions scattered at  $45^\circ$  at a distance of 22 mm from a 200 nm thick  $\text{Si}_3\text{N}_4$  membrane at the conjugate focus position, (Fig. 2 (a)). The second p-i-n detector D2, could be moved into the sample position to directly measure the beam flux. Detectors D1 and D2 are coupled to standard preamplifier-main amplifiers and feed counter-timers via discriminators set to count pulses above the noise pedestal. First, the fluence is measured directly using the detector D2 placed behind a 250  $\mu\text{m}$  diameter aperture at 5 mm distance

from the exit window. Subsequently, the yield from D2 was used to calibrate the yield from D1 in terms of fluence. The beam is then stopped and the tissue sample moved into position. The irradiation is continued until the end point counts in D1 are reached.

#### 4. Irradiation experiments

In order to determine the operating doses, it is preferable to use thin layers of cells rather than a thick piece of tissue because the small size of cells ( $\approx 10 \mu\text{m}$ ) allows accurate determination of the mean stopping force. It is convenient that the Bragg peak is located within the culture substrate. For 2 MeV protons, ICRP (International Commission on Radiological Protection) skeletal muscle tissue was used as model for stopping [5], the projected range is  $74 \mu\text{m}$  (Table 1). The energy deposition is strongly peaked  $\sim 8$  times that at the surface value close to the projected range (Bragg peak) but down to a depth of  $60 \mu\text{m}$ ,  $dE/dx$  only increases by 50% above the surface value allowing a mean energy approximation to be used in Eq. 1. Over this depth range an average dose of 1 Gy for 2 MeV protons corresponds to a fluence of  $\sim 3.03 \times 10^{10}$  protons  $\text{cm}^{-2}$ . Approximating the cells (typical size  $10\text{--}30 \mu\text{m}$ ) in tissue as packed  $20 \mu\text{m}$  dia. spheres, each cell receives about 9520 proton impingements per Gy. It follows that the cells in the irradiated tissue should be in a thin layer on the substrate not exceeding three monolayers for 2 MeV protons. This increases to seven monolayers for a proton energy of 3.4 MeV (the maximum available from a 1.7 MV tandem accelerator).

The collection of astrocytes was approved by UL Lafayette Institutional Animal Care and Use Committee (Protocol ref. 2016-8717-031). Astrocytes were derived from the Tg(NesCre) mouse line as described by Smith et al. [13]. Astrocytes were cultured in T25 culture flasks in 5%  $\text{CO}_2$  using a tissue culture incubator at  $37^\circ\text{C}$ , in DMEM-F12 (Dulbecco's Modified Eagle Medium/Nutrient Mixture F-12) media (Thermo Fisher, 10565042, Waltham, MA) with 5% Fetal Bovine Serum (Thermo Fisher 16140071) and Antibiotic-Antimycotic (Thermo Fisher 15240062). When the cells reached 80–90% confluence (1–2 weeks), they were trypsinized with 0.25% Trypsin/EDTA (Ethylenediaminetetraacetic acid) (Thermo Fisher Scientific) and plated at a density of 50,000 cells per coverslip onto square 22 mm German glass coverslips (Deutsche Spiegelglas 633075, Carolina Biological, Burlington, NC) that were coated with poly-D-lysine (PDL) (Sigma Aldrich P0899, St. Louis, MO).

The low dose (1 and 3 Gy) irradiations with 2 MeV protons were performed in the ultra-low fluence facility with short irradiation times at relatively high flux ( $< 3 \text{ min}$ ,  $1.7 \times 10^8$  protons  $\text{cm}^{-2}\text{s}^{-1}$ ) without the growth-medium present. The flux can be easily reduced by a 100-fold by decreasing the objective and/or collimator apertures. Additionally, high-dose (80 and 600 Gy) irradiations were carried out using a 0.5 mm diameter 2 MeV proton beam in a conventional large-area irradiation facility [14].

Control and irradiated astrocytes were stained with the intracellular  $\text{Ca}^{2+}$  indicator 4  $\mu\text{M}$  Fluo 3 AM in a 3  $\mu\text{M}$  Pluronic 127

(nonionic, surfactant polyol)(Biotum 59000)- 2 mM DMSO (dimethyl sulfoxide) (Sigma Aldrich D2650) HBSS (Hank's Balanced Salt Solution) buffer solution for 20 minutes at  $37^\circ\text{C}$ . Cells were rinsed once with 1% FBS (fetal bovine serum) in HBSS and 4 rinses of HEPES ((4-(2-hydroxyethyl)-1-piperazineethanesulfonic acid) buffer. The coverslip was inverted on top of a 3D-printed imaging chamber containing HEPES buffer, and incubated at  $37^\circ\text{C}$  for 10 minutes, so that the Fluo 3 AM is de-esterified by the cytoplasmic esterases. Astrocytes were imaged with epifluorescence through the coverslip with a Zeiss axio imager microscope, AxioCam MRm camera, and time lapse data collected on Zen software (Zeiss). The SOLA light source (Lumencor) was controlled to 10% output to reduce photobleaching. Image analysis was performed using ImageJ [15].

#### 5. Results and discussion

The astrocytes after 80 Gy (Fig. 4D) of irradiation exhibited acute induction of apoptosis as compared to 0 Gy (Fig. 4A). The 1 Gy and 3 Gy (Fig. 4B) astrocytes (Fig. 4C), respectively, were irradiated in the ultra-low flux facility. The 80 Gy culture was irradiated in a conventional large-area irradiation system. Exposure to 600 Gy resulted in complete necrosis. (Data not shown.) To improve visibility, images in Fig. 4 were imported into Adobe Creative Suite software and coloured. All adjustments to input levels, and brightness/contrast were applied equally to individual images. In all the irradiated cell cultures, abnormal cell morphologies are visible that become more pronounced as the dose increases. This includes a "rougher" appearance of the cytoplasm, large vacuoles within the cells, smaller nuclei, and some instances, cells with multiple nuclei; moreover, fine astrocyte projections that connect with neighboring cells are decreased (Fig. 4). The 80 and 600 Gy results using the large-area irradiation system may be non-uniform and hence these doses should be considered upper limits. In the low-dose experiments, a 1 pA beam diverges behind the conjugate focus to  $\sim 1 \text{ cm}^2$  area delivering MeV proton fluxes of  $\sim 10^6$  ions  $\text{cm}^{-2} \text{ s}^{-1}$ . The biological changes in the cells demonstrate that it can be used to deliver low proton doses that are relevant for simulating space flight conditions. This approach has advantages over other techniques for delivering very-uniform ultra-low flux ion beams to small areas ( $\sim \text{mm}^2$ ). This is important for e.g. irradiation of samples in 96-well microtiter plates, biopsy samples, tissue multi-electrode arrays as well as e.g. neurospheres inside microfluidic circuits that supply nutrients [6] for long-term studies. The small uniform irradiated areas may also be used to deliver spatially varying dose patterns for e.g. studying apoptosis processes. Electromagnetic beam scanning in the  $x$ - $y$  directions is poorly suited to deliver small doses of the order of 10 cGy because technical difficulties with the extremely fast scan frequencies and short exposure times, must be used to achieve uniformly low dose rates (0.24 s/Gy for a 2  $\mu\text{A}$ , 1 mm  $\times$  1 mm 2 MeV proton beam scanned over a 100 mm  $\times$  100 mm area). Combinations of scattering foils and apertures have also been used to spread ion beams [16, 17, 18, 19, 20].

These are best suited for heavy ion beams like C and Ne [19] because the energy lost in the scattering foils limits the ion range in the target when used with 1–3 MeV protons and low energy heavier ions.

## 6. Conclusion

Low MeV proton irradiation facility to deliver ultra-low fluxes of  $10^6$ – $10^{11}$  ions  $\text{cm}^{-2} \text{s}^{-1}$  has been developed at the LAC. The facility is based on post-focus divergence of a focused ion beam in an MeV ion microbeam. Irradiation under BSL-2 conditions in a biocontainment glove box facilitates irradiation of murine and primate tissue using MeV protons and minimises the possibility of infection. The system is also suited for testing radiation-induced parameter changes in de-capped electronic components, optical films etc.

## 7. Acknowledgements

The Jay Dias was supported HJW's start-up fund from the School of Sciences, University of Louisiana at Lafayette. The work was also supported by funding from the Louisiana Accelerator Center.

## References

- [1] I.M. Ghobrial, T.E. Witzig, A.A. Adjei; *Targeting Apoptosis Pathways in Cancer Therapy.*; CA Cancer J Clin. 2009 55(2009)178-194. <https://doi.org/10.3322/canjclin.55.3.178>
- [2] F.A. Cucinotta, M-H. Y. Kim, V. Willingham, K.A. George; *Physical and Biological Organ Dosimetry Analysis for International Space Station Astronauts*; Radiat. Res. 170, 127-138 (2008) <https://doi.org/10.1667/RR1330.1>
- [3] *Space Engineering: Space environment*; (European Cooperation for Space Standardization, Report: ECSS-E-ST-10-04C, 2008)
- [4] CREME Web Site; <https://creme.isde.vanderbilt.edu/>
- [5] J.F. Ziegler, M.D. Ziegler, J.P. Biersack; *SRIM - The stopping and range of ions in matter (2010)*; Nucl. Instrum. Methods. B 268 (2010) 1818-1823. <https://doi.org/10.1016/j.nimb.2010.02.091>
- [6] H. J Whitlow, E. Guibert, P. Jeanneret, A. Homsy, J. Roth, S. Krause, L. Stoppini; A. Roux; *Post-focus expansion of ion beams for low fluence and large area MeV ion irradiation: scaling from the single-event to the system level in human brain tissue and electronics devices*; Nucl. Instrum. Methods. B 404 (2017) 87-91. <http://dx.doi.org/10.1016/j.nimb.2017.01.054>
- [7] D. Mangaiyarkarasi, O. Y. Sheng, M. B. H. Breese, V. L. S. Fuh, E. T. Xioasong; *Fabrication of large-area patterned porous silicon distributed Bragg reflectors*; Optics Express 16, (2008) pp. 12757-12763 <https://doi.org/10.1364/OE.16.012757>
- [8] US Department of Health and Human Services. *Biosafety in Microbiological and Biomedical Laboratories*. 5th ed. 2009. <http://www.cdc.gov/biosafety/publications/bmb15/BMBL.pdf>
- [9] *Occupational Health and Safety in the Care and Use of Nonhuman Primates*; National Research Council (US) Committee on Occupational Health and Safety in the Care and Use of Nonhuman Primates, : National Academies Press (US), Washington (DC); (2003) <https://www.ncbi.nlm.nih.gov/books/NBK43452/>
- [10] Oxford Microbeams Web Site; <http://www.microbeams.co.uk/Products.html>
- [11] G.W. Grime; *WinTRAX: A Raytracing Software Package for the design of multipole focusing systems*; Nucl. Instrum. Methods. B 306 (2013) 76-80. <http://dx.doi.org/10.1016/j.nimb.2012.11.038>
- [12] A. Köhler; *Ein neues Beleuchtungsverfahren für mikrophotographische Zwecke*; Zeitschrift für wissenschaftliche Mikroskopie und für Mikroskopische Technik 10(1893)433-440.
- [13] K.M. Smith, M.E. Maragnoli, P.M. Phull, K.M. Tran, L. Choubey, F.M. Vaccarino; *Fgfr1 inactivation in the mouse telencephalon results in impaired maturation of interneurons expressing parvalbumin.*; PLoS One. 2014 Aug 12;9(8):e103696. <https://doi.org/10.1371/journal.pone.0103696>
- [14] N.T. Deoli, K.H. Hasenstein; *Irradiation effects of MeV protons on dry and hydrated Brassica rapa seeds*, Life Sciences in Space Research 19(2018)24-30. doi: <https://doi.org/10.1016/j.lssr.2018.08.004>
- [15] W.S. Rasband *ImageJ*, U. S. National Institutes of Health, Bethesda, Maryland, USA, <https://imagej.nih.gov/ij/>, 1997-2018.
- [16] P. Scampoli, M. Casale, M. Durante, G. Grossi, M. Pugliese, G. Gialanella; *Low-energy light ion irradiation beam-line for radiobiological studies*. Nucl. Instrum. Methods. B 174 (2001) 337-343. [https://doi.org/10.1016/S0168-583X\(00\)00622-4](https://doi.org/10.1016/S0168-583X(00)00622-4)
- [17] M. Belli, R. Cherubini, G. Galeazzi, S. Mazzucato, G. Moschini, O. Saporà, G. Simone, M.A. Tabocchini; *Proton irradiation facility for radiobiological studies at a 7 MV Van de Graaff accelerator*. Nucl. Instrum. Methods. A 256 (1987) 576-580. [https://doi.org/10.1016/0168-9002\(87\)90304-4](https://doi.org/10.1016/0168-9002(87)90304-4)
- [18] J. Constanzo, M. Fallavier, G. Alphonse, C. Bernard, P. Battiston-Montagne, C. Rodriguez-Lafrasse, D. Dauvergne, M. Beuve; *Radiograaff, a proton irradiation facility for radiobiological studies at a 4MV Van de Graaff accelerator*. Nucl. Instrum. Methods. B 334 (2014) 52-58. <https://doi.org/10.1016/j.nimb.2014.05.005>
- [19] J. Czub, D. Banaś, A. Błaszczak, J. Braziewicz, I. Buraczewska, J. Chojiński, U. Górak, M. Jaskóła, A. Korman, A. Lankoff, H. Lisowska, A. Łukaszek, Z. Szeffiński, A. Wójcik *Biological effectiveness of  $^{12}\text{C}$  and  $^{20}\text{Ne}$  ions with very high LET*, International Journal of Radiation Biology, 84:(2008) 821-829, DOI: 10.1080/09553000802389652
- [20] I.C. Cho, H. Niu, C.H. Chen, W.T. Chou, Y.C. Yu, C.H. Hsu; *A compact biological cell irradiation system with a Van de Graaff accelerator*, Nucl. Instrum. Meth B 315(2013)360-363. doi: <https://doi.org/10.1016/j.nimb.2013.03.042>

## Table

Table 1: Stopping data obtained from the SRIM code [5] and equivalent fluence (protons  $\text{cm}^{-2}$ ) corresponding to dose of 1 Gy for 2 MeV protons.

Material	$dE/dx$ ( keV/ $\mu\text{m}$ )	Ion range	Fluence ( $\text{H}^+ \text{cm}^{-2}$ )
Soft tissue	17.1	71 $\mu\text{m}$	$3.03 \times 10^{10}$
Water	16.4	77 $\mu\text{m}$	$3.04 \times 10^{10}$
Air	0.01	55.3 mm	$5.14 \times 10^{11}$

Figures:

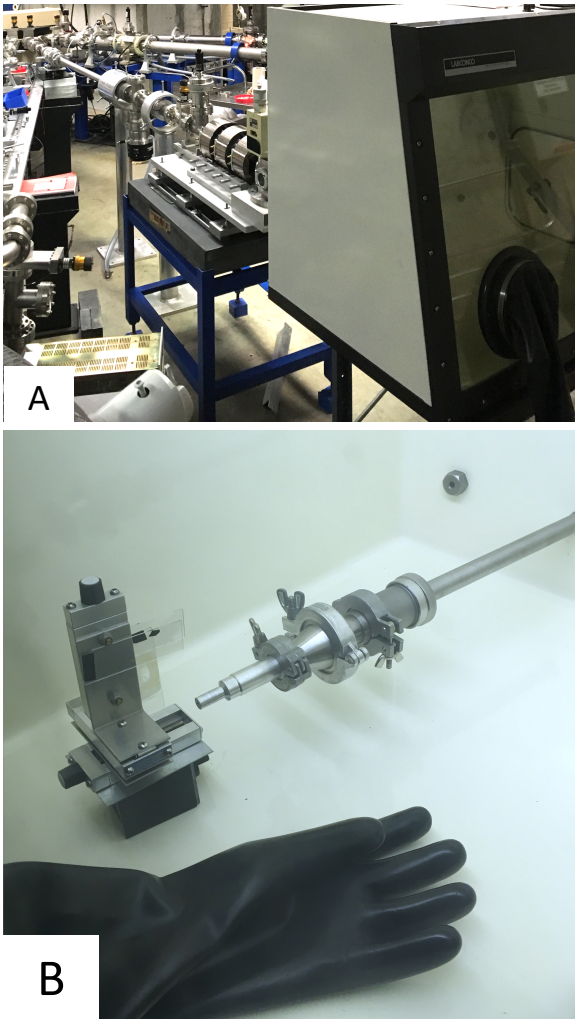


Figure 1: (a) Upstream view of the low-flux irradiation beamline at the LAC showing the beam tube, microprobe lens system, and the glove box in position. (b) Inside view of the glove box with drift section of the beamline equipped with 200 nm thick Si<sub>3</sub>N<sub>4</sub> membrane. For clarity, the sample holder was turned 90° and moved backwards from its normal position.

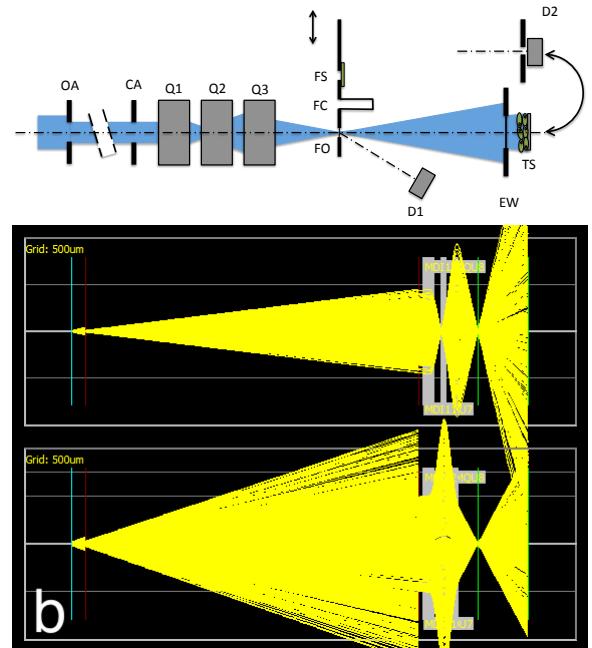


Figure 2: (a) Schematic of the ultra-low fluence irradiation system. Key: OA; objective aperture, CA; collimator aperture, Q1-Q3; magnetic quadrupoles, (FS; fluorescent screen, FC; Faraday cup, FO; scattering foil (Si<sub>3</sub>N<sub>4</sub> membrane), on target stick), EW; exit window, TS; tissue sample on substrate, D1; Si *p-i-n* detector for scattered particles, D2; Si *p-i-n* detector behind precise aperture for direct measurement of ion flux. (b) Screen shot of the ray trajectories from WinTRAX for 0.4 mm diameter collimator aperture CA.

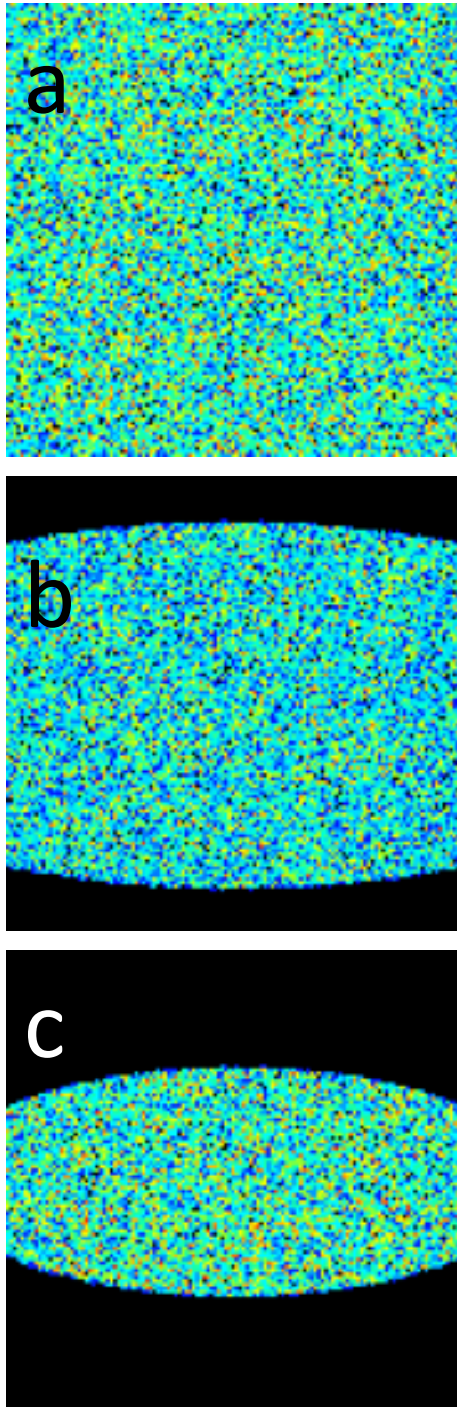


Figure 3: Results of simulations of the intensity distribution using the Win-TRAX code [11] for different collimator apertures. (a) 1 mm diameter (used for the experiments) (b) 0.4 mm diameter and (c) 0.25 mm diameter.

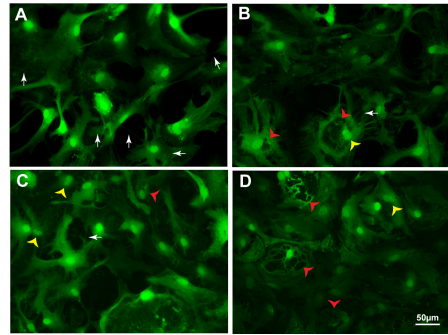


Figure 4: Effect of 2.0 MeV  $H^+$  ions into cultured murine hypothalamic astrocytes (A) 0 Gy, (B) 1 Gy, (C) 3 Gy, and (D) 80 Gy. The white arrows denote fine projections between cells, red arrowheads denote large vacuoles, yellow arrowheads denote cells with two nuclei.